Simultaneous excitation of the snake-like oscillations and the m/n = 1/1 resistive interchange modes around the iota = 1 rational surface just after hydrogen pellet injections in LHD plasmas

journal or publication title	Physics of Plasmas
volume	25
number	1
page range	012507
year	2018-01-10
URL	http://hdl.handle.net/10655/00012785

doi: 10.1063/1.5003058

Simultaneous excitation of the snake-like oscillations and the m/n = 1/1 resistive interchange modes around the iota = 1 rational surface just after hydrogen pellet injections in LHD plasmas

T. Bando[1,a)], S. Ohdachi[1,2], Y. Suzuki[1,2], R. Sakamoto[1,2], Y. Narushima[1,2], Y. Takemura[1,2], K. Y. Watanabe[1], S. Sakakibara[1,2], X. D. Du[3], G. Motojima[2], K. Tanaka[2], T. Morisaki[2], and LHD Experiment Group[2]

[1]*SOKENDAI (The Graduate University for Advanced Studies), 322-6 Oroshi-cho, Toki 509-5292, Japan*

[2]*National Institute for Fusion Science, National Institutes of Natural Sciences, 322-6 Oroshi-cho, Toki 509-5292, Japan*

[3]*University of California Irvine, Irvine, CA 92697, USA*

Abstract

Two types of oscillation phenomena are found just after hydrogen ice pellet injections in the Large Helical Device (LHD). Oscillation phenomena appear when the deposition profile of a hydrogen ice pellet is localized around the rotational transform $\iota = 1$ rational surface. At first, damping oscillations (type-I) appear only in the soft X-ray (SX) emission. They are followed by the second type of oscillations (type-II) where the magnetic fluctuations and density fluctuations synchronized to the SX fluctuations are observed. Both oscillations have poloidal/toroidal mode number, $m/n = 1/1$. Since the type-II oscillations appear when the local pressure is large and/or the local magnetic Reynold's number is small, it is reasonable that type-II oscillations are caused by the resistive interchange modes. Because both types of oscillations appear simultaneously at slightly different locations and with slightly different frequencies, it is certain that type-I oscillations are different from type-II oscillations, which we believe is the MHD instability. It is possible that type-I oscillations are caused by the asymmetric concentration of the impurities. The type-I oscillations are similar to the impurity snake phenomena observed in Tokamaks though type-I oscillations survive only several tens of milliseconds in LHD.

I. INTRODUCTION

"Snake" oscillation is one of the important but not well understood phenomena related to transports in fusion plasmas. The snake-like oscillation was first found in the JET tokamak after hydrogen pellet injections[1]. The name of "snake" is associated with the shape in space time plot of oscillation of soft X-ray (SX) emission, induced by the rotation of helical structure. The helical structure is a quite localized region extending along the magnetic field line having $m/n = 1/1$ structure. Though snakes are localized on the $q = 1$ rational surface they survive the sawtooth crashes. Several theoretical models, such as the generation of the magnetic island by the excitation of the tearing mode[2] or helical core equilibrium[3], have been proposed. However, no model can fully explain the characteristics of snakes observed in the experiments. On the other hand, snakes having $m/n = 1/1$ structures induced by the impurity concentration are reported in several devices, such as the Doublet-III[4], PBX[5], or the Alcator-C mod device[6].

[a)]Electronic mail: bando.takahiro@nifs.ac.jp

Because these types of snake-like oscillation phenomena are reported in most tokamaks[1,7,8], RFPs[9], and a spherical torus[10], it may be a common feature in magnetic confinement devices. Snakes are not only interesting phenomena, they also are quite important phenomena to understand the mechanism of the formation since, in the present ITER experimental scenarios, the q = 1 rational surface is located in the middle of plasmas and the behavior of the impurity concentration is quite important for realizing fusion reactors.

Large Helical Device (LHD) is a Heliotron-type device with superconducting helical coils having winding numbers of 2/10. The major radius is 3.9 m and averaged minor radius is 0.6m[11]. In LHD, hydrogen pellet injections are one of important ways to provide fuel to the core of plasmas. The pressure profile is changed significantly by a hydrogen pellet injection in LHD. Figure 1 shows the profile of (a) electron pressure, (b) electron density, and (c) electron temperature before and after a pellet injection. These profiles were measured by Thomson scattering measurement[12]. The red circles and blue triangles show the profiles before and after the pellet injection, respectively. The green dashed line indicates the normalized minor radius around the rotational transform $\iota = 1$ surface. The electron pressure gradient around the $\iota = 1$ radius increases by about 50 % with the increase of the electron density and the decrease of the electron temperature as shown in Fig. 1. It is also known that the density profile becomes peaked gradually after the pellet injection. With such a steeper pressure gradient, pressure-driven MHD instabilities can be unstable in LHD plasmas[13, 14].

Oscillations just after the ice pellet injection were reported in previous study[15, 16]. Detailed analyses of those oscillations have revealed that there are two types of oscillations. In this article, the observations of the two types of oscillations induced by hydrogen pellet injections in LHD are reported. The first type of damping oscillations (type-I) appear only in SX emission when the pellet is ablated mainly around ι = 1 surface. Type-I oscillations are sometimes followed by the second type of oscillations (type-II) with the magnetic fluctuations and density fluctuations synchronized to the SX emission fluctuations. As discussed in the following sections, it is possible that the type-I oscillations are impurity snake phenomena and the type-II oscillations are m/n = 1/1 resistive interchange modes induced by steep pressure gradients by pellet injections.

This article is organized as follows. In section II, the experimental setup and analysis methods are explained. In section III, characteristics of type-I and type-II oscillation just after hydrogen pellet injections are introduced in detail. In section IV, the discussion regarding two types of oscillation is given. The study is summarized in section V.

II. Experimental setup and analysis methods

The experimental condition in which type-I and type-II oscillations are observed is as follows. The vacuum magnetic axis R_{ax} is 3.6 m and the aspect ratio A_p is the standard ratio, $A_p = 5.8$. In this condition, the ι profile monotonically increases as the normalized minor radius (ρ) increases. In the vacuum magnetic configuration, $\iota = 0.38$ surface is located on the magnetic axis and the $\iota = 1$ rational surface is located around $\rho = 0.85$.

Figure 2 shows a schematic view of diagnostics used in this article. The hydrogen ice pellet injector[17] is located at the toroidal angle of $\phi = 288$ degrees. The hydrogen pellet injector can inject pellets repeatedly from the outboard side of the plasma. The speed of the injected pellet is 1000~1400 m/s. The numbers of hydrogen atoms in pellets used in this study are 1×10^{21}, 1.5×10^{21} or 2×10^{21}. There is a Hα detector located near the pellet injector. The time evolution of the relative amount of the ablation of pellets can be measured by the Hα detector. The SX detector array systems viewing the whole poloidal cross section are installed at several locations, ϕ=108, 162, and 270 degrees[16, 18, 19]. Figure 2(c) shows the sight lines of the main SX array installed at $\phi = 270$ degrees. The CO_2 laser imaging interferometer is located at $\phi = 90$ degrees[20]. There are three groups of sight lines and there are two gaps between the groups. The sight lines of the CO_2 laser imaging interferometer is shown in Fig. 2(b). Though the SX emission signals and the line integrated electron density obtained with the CO_2 laser imaging interferometer include line integrated effect, it is sufficient to identify structures of oscillation reported in this study. Magnetic probes[21] are used to determine the poloidal and toroidal mode numbers of the MHD activities. It is noted that the ECE measurement cannot be used due to the cutoff of the wave caused by the abrupt ramp-up of the electron density by pellet injections.

In the following subsections, Singular Spectrum Analysis[22] (SSA) is used to obtain fluctuation component of SX emission signals. SSA is a technique based on Singular Value Decomposition (SVD) and effective for separating fluctuation component from signals when trend component is also changing. SSA shows better performance compared with the conventional FFT method.

The flux surfaces and ι profiles used in this study are estimated by fixed-boundary VMEC code[23] assuming pressure profiles similar to the experimentally observed pressure profiles. The toroidal current is not included in the equilibrium calculations.

III. Characteristics of type-I and type-II oscillation

Figure 3 shows typical time evolution of several kinds of signals when oscillation phenomena are observed. (a) SX emission measured at ϕ =270 degrees, (b) the line integrated electron density, n_eL, obtained with the CO_2 laser imaging

interferometer, (c) the magnetic fluctuations, and (d) the Hα emission. Two signals in Fig. 3(a) show the SX emission from red solid and blue dashed sight lines shown in Fig. 2(c) with the same colors. The minor radii viewed by the red and blue sight lines are about $\rho = 0.89$ and 0.78, respectively. The hydrogen pellet is injected at 3.743s then ablated for about 390μs as shown in Fig. 3(d). Figure 4 shows (a) the flux surface at a horizontally elongated poloidal cross section, where the pellet is injected, and (b) the ι profile. The pressure profile in the calculation of the VMEC is similar to the profile after the pellet is injected. In Fig. 4(a), the green region roughly indicates the flux surface at $\iota = 1$. The deposition profile of the pellet, which is estimated by the time evolution of the Hα signal and the speed of the injected pellet, is shown by the blue line in Fig. 4(b). It is clear that the pellet is ablated around the $\iota = 1$ surface. The pressure gradient around the $\iota = 1$ surface thereby becomes steeper. The pressure gradient can be the driving force of resistive interchange modes usually observed in LHD plasmas as mentioned in section I.

The time for ablation is 3-7 times longer than the characteristic time of ion acoustic waves, $2\pi R_{ax}/v_s$. v_s is the speed of the ion acoustic waves and calculated as $(Te/m_i)^{0.5}$. m_i is the mass of the proton. The two types of oscillations reported in this article seem to appear after the transient states of the ion acoustic waves.

After the ablation of the pellet, the damping oscillation was observed on SX emission signals. Hereafter, we refer the damping oscillation as type-I oscillation. The peak of the fluctuation level ($\delta I_{SX}/I_{SX}$) of the type-I oscillation is located around $\rho = 0.78$ on SX emission signals as shown in Fig. 3(a). No coherent electron density and magnetic fluctuation are observed in type-I phase as shown in Fig. 3(b) and (c). After the type-I oscillation attenuates, another type of oscillation (type-II) appears in the SX emission signals viewing at approximately around $\rho = 0.89$, the line integrated density around $\rho = 0.84$, and the magnetic fluctuation measurement. The peak of the fluctuation level of type-II oscillation on SX emission is slightly on the outside of the radii where the type-I oscillation locates. The fluctuation amplitude of the type-I oscillations is usually larger than that of the type-II oscillations. In the case of the Fig. 3(a), they are 60% and 15%, respectively. It is noted that the ρ values, where fluctuation levels are high, are slightly different between the SX detector array system and the CO2 laser imaging interferometer because the shapes of poloidal cross sections viewed by two systems are different as shown in Fig. 2(c) and (b).

Figure 5 shows time evolution of (a) SX emission signals viewing $R = 4.05$ m ($\rho = 0.71$) which shows the damping type-I oscillation of (b) the fluctuation component of SX emission as a function of time and the chord location, and (c) the ι profile and the magnetic shear on the vertically elongated cross section. In Fig. 5, type-II oscillation is not observed. Rotation of the $m = 1$ structure, which is similar to snakes, is clearly observed in Fig. 5(b). The peaks of the "snake" structure is localized around or slightly inside the $\iota = 1$ surface as shown in Fig. 5(b) and (c). The shear around the $\iota = 1$ surface appears to be weak

.

to satisfy inequality (6) in Ref. 2, which is a proposed condition to form a snake-like structure. Figure 6 shows SX emission signals from chords viewing around the $\iota = 1$ surfaces at different toroidal angles, $\phi = 108$, 162, and 270 degrees, respectively at the same pellet injection as that in Fig. 5. The toroidal mode number is estimated to be unity from the phase difference between each signal. Since the fluctuation level is almost constant, it is quite likely that this snake-like structure is extending toroidally and continuously.

The observed toroidal rotation directions of the snake-like type-I structure are the opposite direction of the direction of the magnetic field. Though the poloidal rotation direction cannot be detected with SX diagnostics viewing poloidal cross sections from one direction, the result of 2D-SX camera viewing the plasma tangentially indicates that the poloidal rotation direction is the electron diamagnetic direction[16]. Poloidal rotations to electron diamagnetic directions are the same as that of resistive interchange modes observed in LHD[24]. The frequency of the snake-like oscillation varies from 300 Hz to 700 Hz in discharges which have been analyzed. The frequency is not changing during the damping process. The frequencies are the same order as the electron diamagnetic frequency around $\iota = 1$ surface.

The stability of the Mercier modes is considered with the Mercier parameter, D_M. When $D_M > 0$, Mercier modes are marginally stable. In the case of figure 5, D_M is 0.025 around R=4.03m where the peak of type-I oscillation is observed. Therefore, type-I oscillation is not a Mercier mode.

The observed duration time of the snake-like oscillation is up to 0.03 s. The duration time of the type-I oscillation is not as long as the snakes in tokamaks. If we evaluate the decay time of the column whose diameter is 0.1m with the diffusion coefficient $D = 0.5$ m^2/s, which is typical diffusion coefficient for the bulk plasma in LHD[25], the decay time is about 0.01s. Diffusive process from the pellet-induced asymmetric profile may be the cause of the decay of the amplitude of the type-I oscillation.

The SX emission depends on the electron temperature, the electron density, and the impurity density. There are no density fluctuations in the type-I phase as shown in Fig. 3(b). If the electron temperature fluctuates, the electron density should be also changed to maintain the electron pressure constant on a flux tube. Since the change in the electron density and the electron temperature is too small to explain the change in the SX emission, asymmetric concentration of the impurity is one candidate to explain the oscillations in the SX emission. Figure 7 shows (a) the SX emission signal viewing around the $\iota = 1$ surface and (b) the line emission of FeXVI measured by a VUV spectrometer. The wave length of the line emission is 33.5 nm. This observation supports the view that the fluctuations in the SX emission are caused by impurities.

A. Type-II oscillation accompanied by magnetic fluctuations

The type-II oscillation is accompanied by the electron density and magnetic fluctuation as well as the fluctuations in SX emission. The frequencies of type-II oscillation are the same order as the frequencies of type-I oscillation. The mode number of the type-II oscillations can be determined by the magnetic probes. It is $m/n = 1/1$. These oscillations are considered to be the resistive interchange modes from the discussions below. As explained in section I, resistive interchange modes can be unstable with steeper pressure gradients induced by pellet injections. Figure 8 shows the relationship between the local magnetic Reynold's number, S, and the local β value around $\iota = 1$ surfaces obtained with and without type-II oscillations. Red and blue points indicate data with and without type-II oscillations, respectively. Type-II oscillations appear when the local pressure is large and/or the local Reynold's number is small though the trend is slight. The slight trend may be due to errors of estimation of $\iota = 1$ surfaces. The saturation level of the mode amplitude for resistive interchange modes is proportional to $S^{-1/3}$ in LHD[26]. It is clear that the type-II oscillations appear when the resistive interchange mode is unstable. Besides, the observed rotation directions (electron diamagnetic drift direction) are also consistent with the rotation direction of the resistive interchange mode observed in LHD[24].

B. Coexistence of snake-like type-I oscillations and resistive interchange modes

There are many observations that type-I oscillations and type-II oscillations, which may be resistive interchange modes, are excited simultaneously. Figure 9 shows the time evolution of (a) magnetic fluctuations, (b) SX emission from two channels, (c) fluctuation component of SX emission signals, and (d) the ι profile. In Fig. 9(b), the blue dashed the line and red solid line show type-I and type-II oscillations, respectively. In Fig. 9, the pellet is ablated at 3.8435 s and the type-I oscillation appears. The type-II oscillation appears from 3.847 s and overlaps with each other. These oscillations are not Mercier modes because D_Ms are greater than 0 around peaks of type-I and type-II oscillation.

The mode width of the resistive interchange modes are usually quite localized around $\iota = 1$ surfaces in LHD. However, peaks of snake-like type-I oscillation are localized slightly on the inner side of the radii where resistive interchange modes are observed as shown in Fig. 9 (c). In addition, these have different frequencies. The frequencies of type-I and type-II oscillations are approximately 680 Hz and 490 Hz in Fig. 9 (b). These observations suggest that the snake-like type-I oscillation are different from resistive interchange modes though snake-like type-I oscillation has the mode structure closed to $m/n = 1/1$.

IV. Discussion

Since both types of oscillation appear simultaneously at slightly different locations and with slightly different frequencies, it is certain that type-I oscillations are different from type-II oscillations, which we believe are the MHD instabilities. It is expected that density fluctuations cause type-I oscillation since there should be localized density perturbations due to pellet ablation. However we have not observed oscillation of the density in type-I phases experimentally. One of possible explanations is that oscillations observed in SX emission is caused by the asymmetric concentration of the impurity and the rotation of the plasma as discussed below. In LHD, the impurity transport is quite sensitive to the collisionality of the plasma[27]. Moreover, recent LHD experiment revealed that the strong gradient of the electron density causes the outward transport of impurities[28]. Then it is possible that impurity ions in the core plasma are transported to the outward direction by the formation of the steep electron density gradient by the ablation of the pellet. The accumulated impurity may form a strong emission layer inside the $\iota = 1$ rational surface as shown in Fig. 10. Figure 10 is a schematic drawing of the radiation layer at a vertically elongated poloidal cross section. The solid green line is the $\iota = 1$ surface and the dashed green line is the deformed $\iota = 1$ surface with $m = 1$ deformation. Then the red-colored region is the region where impurity ions accumulate with $m = 1$ structure slightly on the inner side of $\iota = 1$ surface. The red and blue sight lines are the same as the sight lines for SX emission signals in Fig. 3(a). The role of the rational surface of $\iota = 1$ in impurity transport has not been clarified. However, when the pellet is deposited deeply inside the plasma, similar damping oscillations are observed near $\iota = 1/2$ rational surfaces, as well. Therefore, the existence of the low-number rational surface may be necessary for the snake-like type-I oscillations.

The origin of the poloidal and toroidal asymmetry of the impurity density, which may cause the oscillation in laboratory frame, is an open issue. However, similar phenomena is reported in another helical device, TJ-II Stellarator. Damping oscillation just after the pellet injection having $m = 1$ mode structure was found in the TJ-II Stellarator[29]. This phenomenon was explained by the change of the friction force due to sudden change of plasma parameters induced by a pellet injection. The equilibrium of the LHD is also a three dimensional equilibrium. Similar 3D effects may be a candidate to explain the generation of the poloidal asymmetry of the impurity profile.

Note that the Geodesic Acoustic Mode (GAM) is also a candidate of the type-I oscillation because pellet injections can bring the momentum into plasmas. The possibility of excitations of GAMs should be also examined in the future.

V. Summary

In this article, two types of oscillation phenomena observed just after the pellet injections in LHD are reported. Type-I snake-like oscillation is observed only in SX emission just after ablation of injected pellets when the pellets are ablated mainly around $\iota = 1$ rational surface. The snake-like oscillation may be caused by asymmetric concentration of impurities, since coherent oscillation of line emission of FeXVI is observed, as well. Type-II oscillation, which is the resistive interchange mode, then sometimes appears. Because both types of oscillations appear simultaneously at slightly different locations and with slightly different frequencies, it is certain that type-I oscillations are different from type-II oscillations. In order to narrow the physical models of the snake, our observation that two types of oscillation are excited simultaneously may play an important role.

ACKNOWLEDGMENTS

The authors would like to thank Professor Emeritus. K. Toi, Prof. L. Q. Hu, Dr. H. Tsuchiya, Dr. R. Ishizaki, Dr. M. Goto, Dr. H. L. Huang, Dr. N. Tamura, Dr. C. Suzuki, and Dr. H. Funaba for many fertile discussions. This work was supported by NIFS budget code ULPP021, 028 and is also partially supported by the Ministry of Education, Science, Sports and Culture Grant-in-Aid for Scientific Research 26249144, by the JSPS-NRF-NSFC A3 Foresight Program (NSFC: No.11261140328, NRF: No. 2012K2A2A6000443), and by NIFS/NINS under the project Formation of International Scientific Base and Network.

REFERENCES

[1]A. Weller, A. D. Cheetham, A. W. Edwards, R. D. Gill, A. Gondhalekar, R. S. Granetz, J. Snipes, and J. A. Wesson, Phys. Rev. Lett. **59**, 2303 (1987).

[2]J. A. Wesson, Plasma Phys. Control. Fusion **37**, A337 (1995).

[3]W.A. Cooper, I.T. Chapman, O. Schmitz, A.D. Turnbull, B.J. Tobias, E.A. Lazarus, F. Turco,M.J. Lanctot, T.E. Evans, J.P. Graves, D. Brunetti, D. Pfefferle, H. Reimerdes,O. Sauter, F.D. Halpern, T.M. Tran, S. Coda, B.P. Duval, B. Labit, A. Pochelon, M.R. Turnyanskiy, L.Lao, T.C. Luce, R. Buttery, J.R. Ferron, E.M. Hollmann, C.C. Petty, M. van Zeeland,M.E. Fenstermacher, J.M. Hanson and H. Lutjens, Nucl. Fusion **53**, 073021 (2013).

[4]Jahns G.L. Jahns, S. Ejima, R.J. groebner, N.H. brooks, R.K. Fisher, C.L. Hsieh, T.S. Taylor, and J.C. Wesley, Nucl. Fusion **22**, 1049 (1982).

[5]K. Ida, R. J. Fonck, R. A. Hulse and B. Leblanc, Plasma Phys. Controlled Fusion **28**, 6 (1986).

[6]L. Delgado-Aparicio, L Sugiyama, R. Granetz, D. Gates, J. Rice, M.L. Reinke, W. Bergerson, M. Bitter, D.L. Brower, E. Fredrickson, C. Gao, M. Greenwald, K. Hill, A. Hubbard, J. Irby, J.W. Hughes, E. Marmar, N. Pablant, S. Scott, R. Wilson, S. Wolfe and S. Wukitch, Nucl. Fusion **53**, 043019 (2013).

[7]Y. Kamada, T. Ozeki, and M. Azumi, Phys. Fluids B **4**, 124(1992).

[8]Xingjia Yao, Jiansheng Hu, Liqing Xu, Zong Xu, Yue Chen, Changzheng Li, Haiqing Liu, Hailing Zhao, Yanmin Duan, Tonghui Shi, Wei Shen and EAST Team, Plasma Phys. Control. Fusion **58**, 105006 (2016).

[9]P. Martin, L.Marrelli, G. Spizzo, P. Franz, P. Piovesan, I. Predebon, T. Bolzonella, S. Cappello, A. Cravotta, D.F. Escande, L. Frassinetti, S. Ortolani, R. Paccagnella, D. Terranova, the RFX team, B.E. Chapman, D. Craig, S.C. Prager, J.S. Sarff, the MST team, P. Brunsell, J.-A. Malmberg, J. Drake, the EXTRAP T2R team,Y.Yagi, H. Koguchi, Y. Hirano, the TPE-RX team, R.B. White, C. Sovinec, C. Xiao, R.A. Nebel8 and D.D. Schnack, Nucl. Fusion **43**, 1855 (2003).

[10]J.E. Menard, R.E. Bell, E.D. Fredrickson, D.A. Gates, S.M. Kaye, B.P. LeBlanc, R.Maingi, S.S. Medley,W.Park, S.A. Sabbagh, A. Sontag, D. Stutman, K. Tritz, W.Zhu and the NSTX Research Team, Nucl. Fusion **45**, 539 (2005)

[11]A. Komori, H. Yamada, S. Imagawa, O. Kaneko, K. Kawahata, K. Mutoh, N. Ohyabu, Y. Takeiri, K. Ida, T. Mito, Y. Nagayama, S. Sakakibara, R. Sakamoto, T. Shimozuma, K. Y.Watanabe, and O. Motojima for LHD Experiment Group, Fusion Sci. Technol. **58**, 1 (2010) .

[12]I. Yamada, H. Funaba, R. Yasuhara, H. Hayashi, N. Kenmochi, T. Minami, M. Yoshikawa, K. Ohta, J. H. Lee, and S. H. Lee, Rev. Sci. Instrum. **87**, 11E531 (2016).

[13]S. Ohdachi, K. Toi, G. Fuchs, S. Sakakibara, K. Y.Watanabe, Y. Narushima, K. Narihara, K. Tanaka, T. Tokuzawa, S. Inagaki, Y. Nagayama, F.Watanabe, K. Kawahata, K. Komori and the LHD Exprimental Group, "Two–Dimensional Structure of MHD Instabilities and their Non–Linear Evolution in the Large Helical Device." Proc. 21th IAEA Fusion Energy conference, Chegdu, China. EX/P8-15 (2006).

[14]S. Ohdachi, K.Y. Watanabe, K. Tanaka, Y. Suzuki, Y. Takemura, S. Sakakibara, X.D. Du, T. Bando, Y. Narushima, R. Sakamoto, J. Miyazawa, G. Motojima, T. Morisaki and LHD Experiment Group Nucl. Fusion **57**, 066042 (2017).

[15]S. Ohdachi, K. Toi, R. Sakamoto, H. Yamada, G. Fuchs, S. Yamamoto, and LHD experiment Group, “Dynamics of Pellet Ablation Clouds Observed in LHD by a Fast-Framing Tangentially Viewing Soft X-Ray Camera”, Proc. 30th Conf. Controlled Fusion and Plasma Physics, St. Petersburg, Russia (2003).

[16]S. Ohdachi, F. Watanabe, S. Yamamoto, K. Toi, C. Suzuki, K. Ida, S. Muto, and LHD Experiment Group, Fusion Sci. Technol. **58**, (2010).

[17]R. Sakamoto, G. Motojima, H. Hayashi, T. Inoue, Y. Ito, H. Ogawa, S.Takami, M. Yokota, and H. Yamada, Rev. Sci. Instrum. **84**, 083504 (2013).

[18]X. D. Du, S. Ohdachi, K. Toi,and LHD Experiment Group, Plasma and Fusion Research **7**, 2401088 (2012).

[19]S. Ohdachi, Ph.D. thesis, Nagoya University, 2003.

[20]K. Tanaka, C. Michael, L. Vyacheslavov, A. Sanin, K. Kawahata, S. Okajima, T. Akiyama, T. Tokuzawa and Y. Ito, Plasma and Fusion Research **2**, S1033 (2007).

[21]S. Sakakibara, H. Yamada, and LHD Experiment Group, Fusion Sci. Technol. **58**, 471, (2010).

[22]Golyandina, Nina, and Anatoly Zhigljavsky. *Singular Spectrum Analysis for time series* (Springer Science & Business Media, 2013).

[23]S. P. Hirshman and J. C. Whitson, Phys. Fluids **26**, 3553 (1983).

[24]Y. Takemura, S. Sakakibara, K. Watanabe, K. Ichiguchi, K. Ida, Y. Suzuki, S. Ohdachi, Y. Narushima, I. Yamada, K. Tanaka, H. Yamada and LHD Experiment Group, Plasma and Fusion Research **8**, 1402123 (2013) .

[25]K. Tanaka, C.Michael, A.L. Sanin, L.N. Vyacheslavov, K. Kawahata, S.Murakami, A.Wakasa, S. Okajima, H. Yamada,M. Shoji, J.Miyazawa, S.Morita, T. Tokuzawa, T. Akiyama,M. Goto,K.Ida,M. Yoshinuma, I. Yamada, M. Yokoyama,

S.Masuzaki, T.Morisaki, R. Sakamoto, H. Funaba, S. Inagaki, M. Kobayashi, A. Komori and LHD Experiment Group, Nucl. Fusion **46**, 110 (2006).

[26]S. Sakakibara,K. Y. Watanabe, Y. Suzuki, Y. Narushima, S. Ohdachi, N. Nakajima, F. Watanabe, L. Garcia, A. Weller, K. Toi, I. Yamada, K. Tanaka, T. Tokuzawa, K. Ida, H. Yamada, A. Komori, O. Motojima and the LHD Experiment Group, Plasma Phys. Controlled Fusion **50**, 124014 (2008).

[27]Y. Nakamura, N. Tamura, M. Yoshinuma, C. Suzuki, S. Yoshimura, M. Kobayashi, M. Yokoyama, M. Nunami, M. Nakata, K. Nagaoka, K. Tanaka, B.J. Peterson, K. Ida, M. Osakabe, T. Morisaki and the LHD Experiment Group, Nucl. Fusion **57** 056003 (2017).

[28] X.L. Huang, S. Morita, T. Oishi, I. Murakami, M. Goto, H.M. Zhang, Y. Liu and The LHD Experiment Group , Nucl. Fusion **57**, 086031 (2017).

[29]J. A. Alonso, J. L. Velasco, I. Calvo, T. Estrada, J. M. Fontdecaba, J. M. García-Regaña, J. Geiger, M. Landreman, K. J. McCarthy, F. Medina, B. Ph. Van. Milligen, M. A. Ochando, F. I. Parra, the TJ-II Team1 and the W7-X Team, Plasma Phys. Controlled Fusion **58**, 074009, (2016).

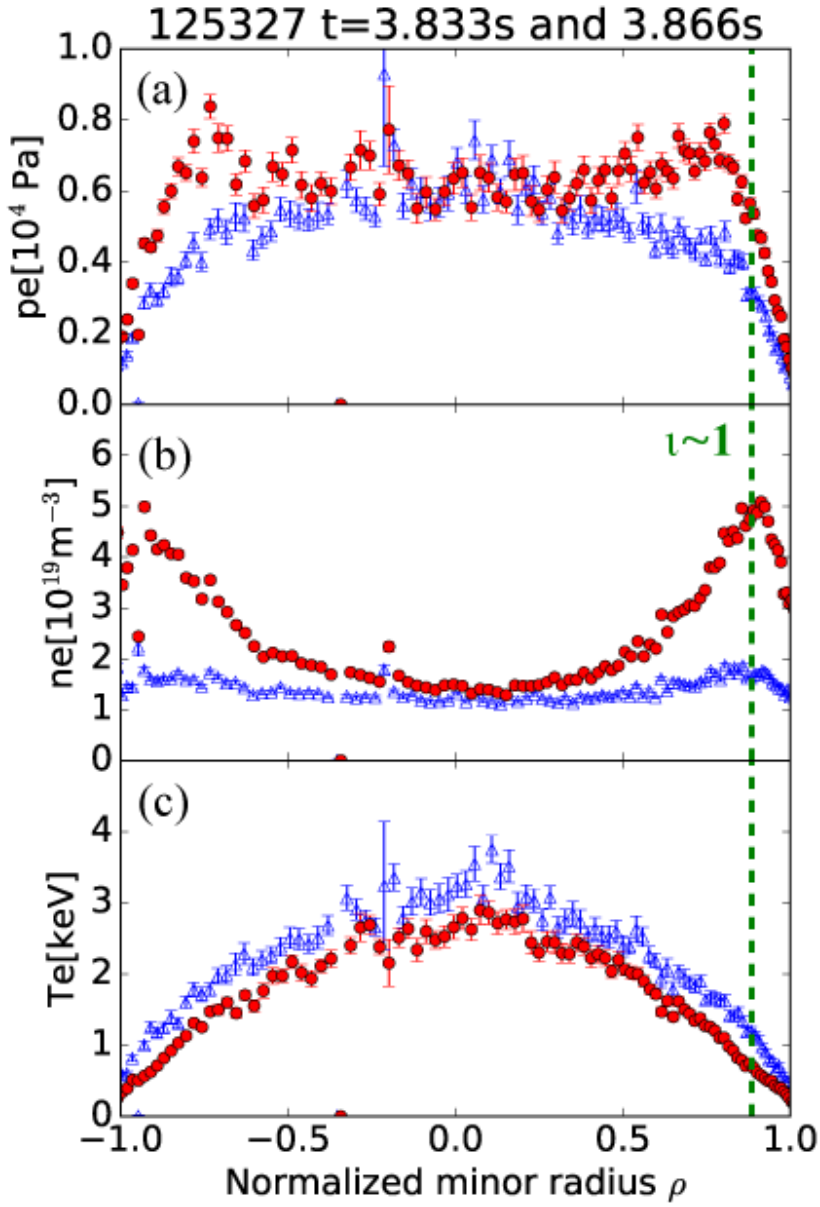

FIG. 1. The profile of (a) electron pressure, (b) electron density, and (c) electron temperature before and after a pellet injection.

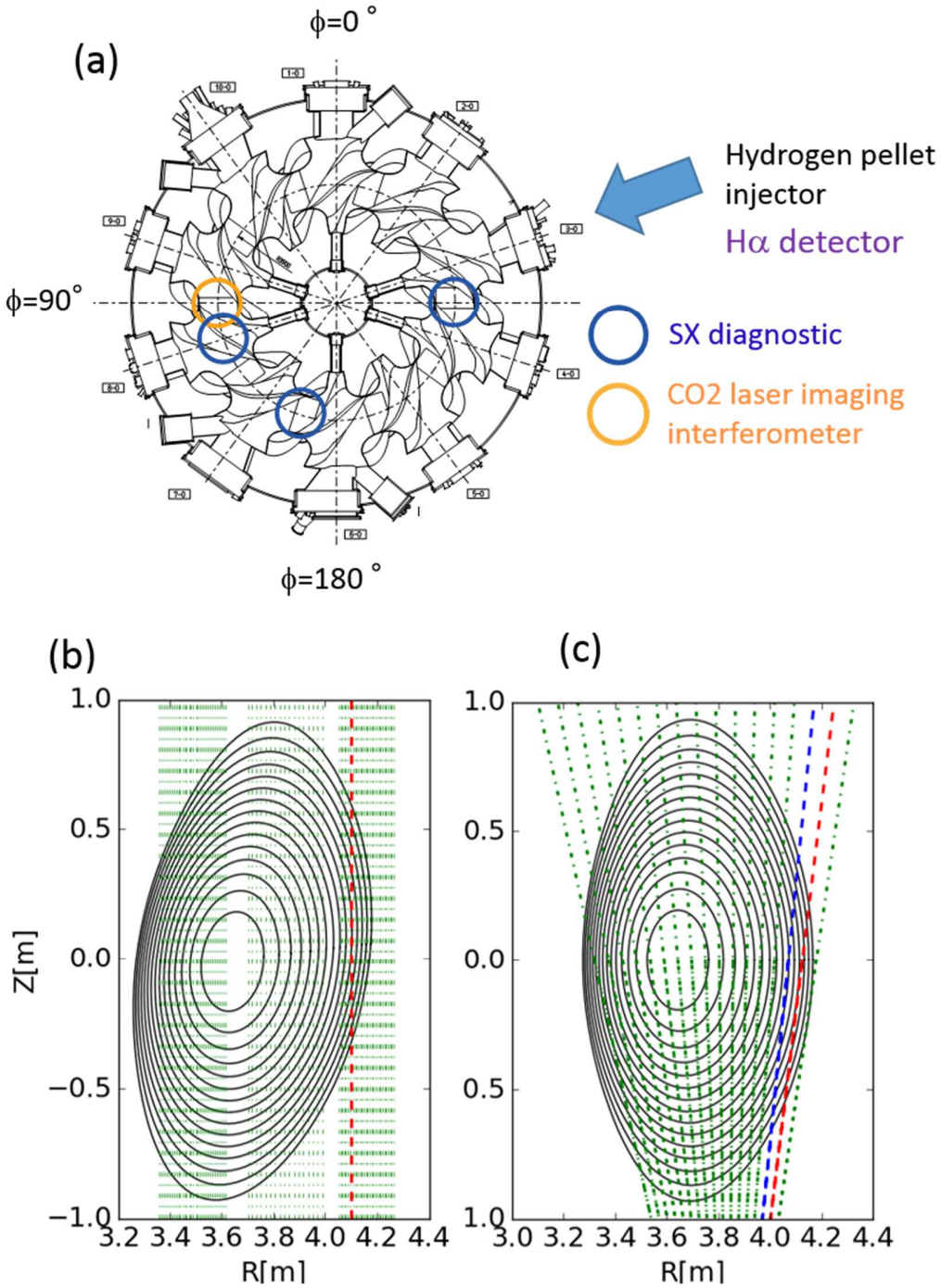

FIG. 2. Figure (a) shows the geometrical information of the diagnostic used to determine spatial structure of modes in this article. Figure (b) shows the sight lines of the CO2 laser imaging interferometer at $\phi = 90$ degrees. Figure (c) shows the sight lines of SX diagnostic installed at $\phi = 270$ degrees. The red dashed sight line in Figure (b) is the red sight line for the signal in Fig. 3(b). The red dashed and blue dashed sight lines in Figure (c) are sight lines for two signals in Fig. 3(a).

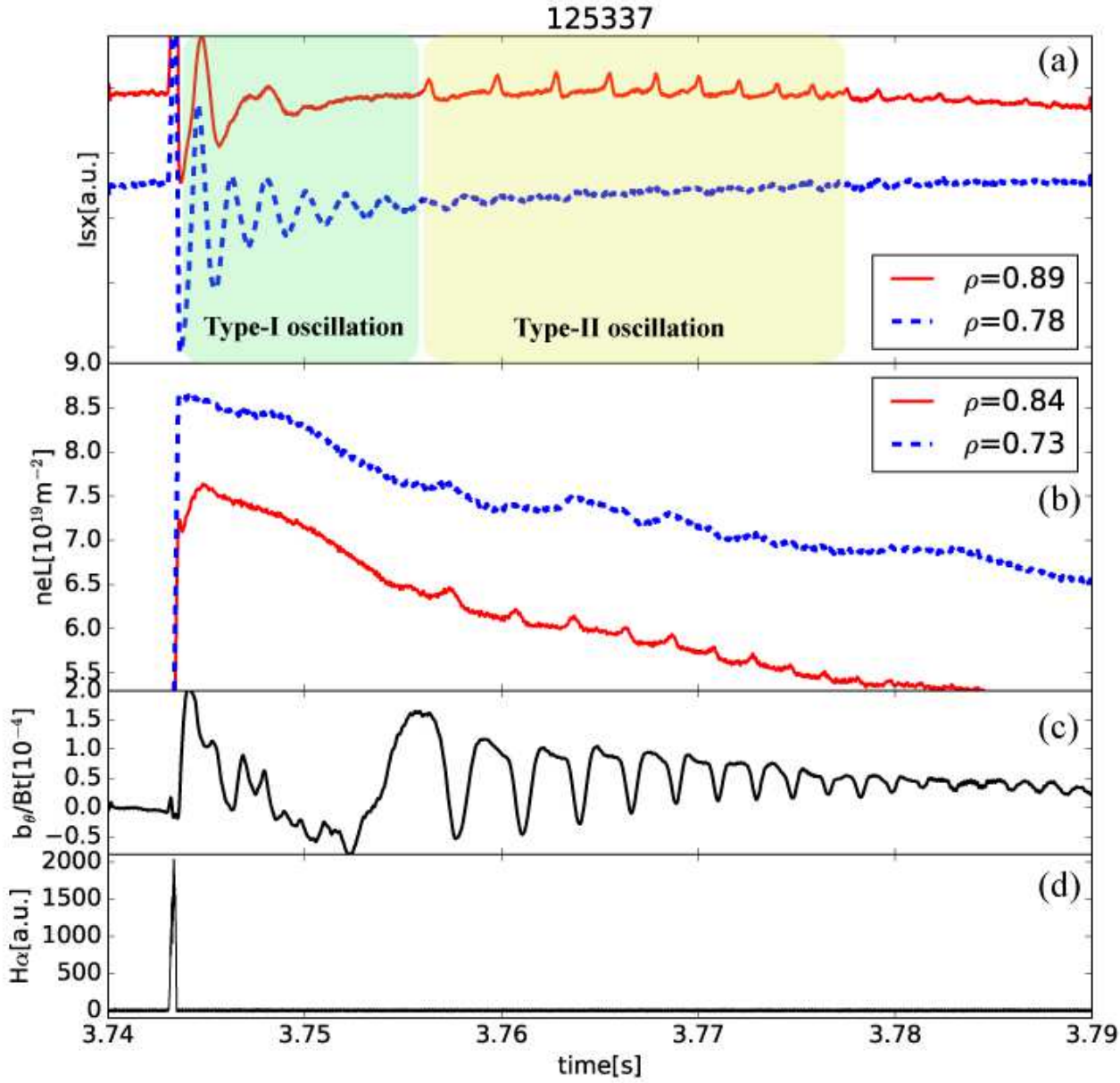

FIG. 3. Typical time evolution of (a) SX emission signals from SX diagnostic at ϕ=270 degrees, (b) line integrated electron density, *neL*, obtained with the CO2 laser imaging interferometer, (c) magnetic fluctuations, and (d) Hα signals when type-I and type-II oscillation.

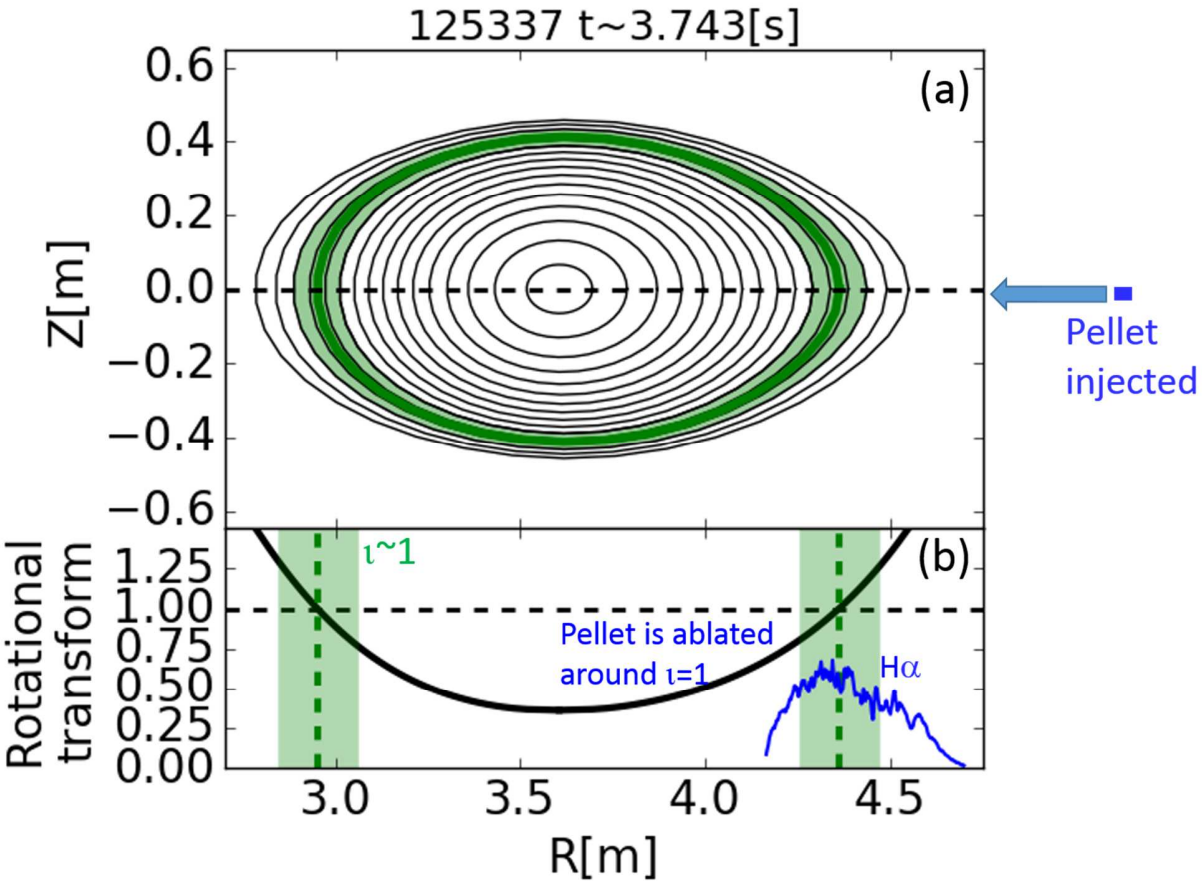

FIG. 4. (a) Flux surfaces at a horizontally elongated poloidal cross section and (b) the ι profile from a VMEC equilibrium assuming the pressure profile after the pellet injection. In figure (a), the green region roughly indicates the location of the $\iota = 1$ rational surface. In figure (b), the blue line means the radial profile of ablated amounts of the pellet estimated by the speed of the injected pellet and the time evolution of Hα signals.

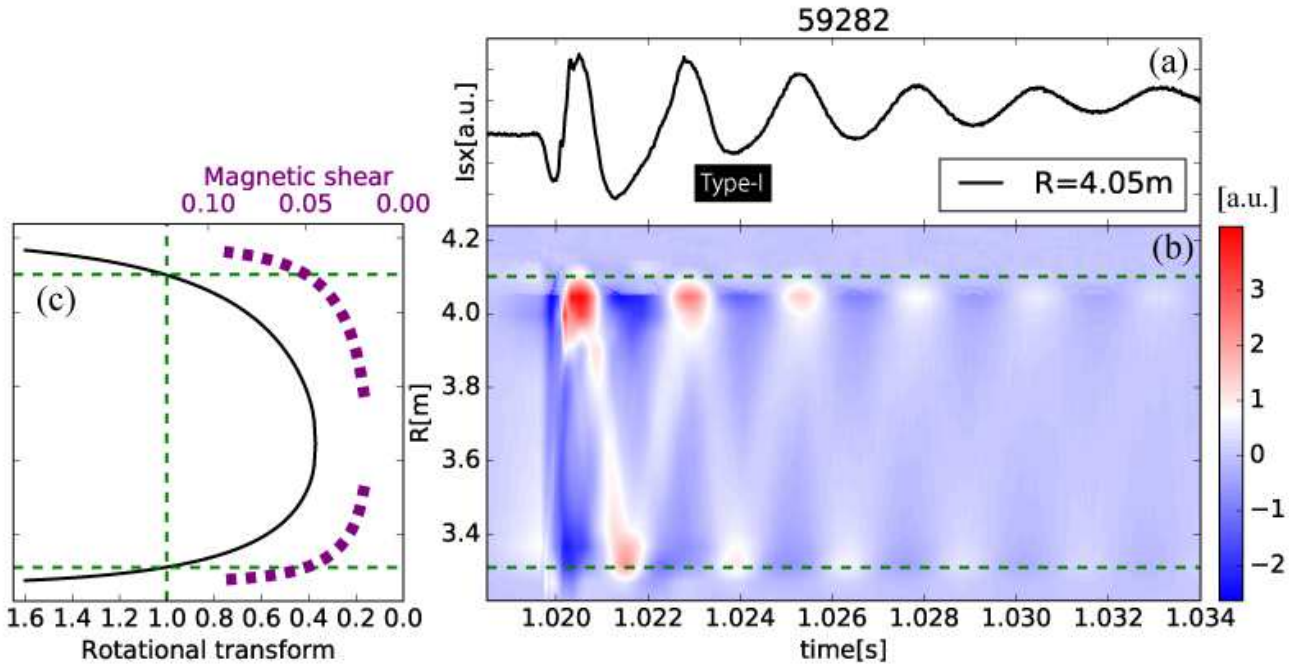

FIG. 5. Time evolution of (a) SX emission signals viewing R= 4.05 m which shows the damping oscillation of the snake structure, (b) the radial profile of fluctuation component of SX emission signals, and (c) the ι profile and the magnetic shear on the vertically elongated cross section. In figure (c), the solid black line is the iota profile and the purple dashed line is the magnetic shear.

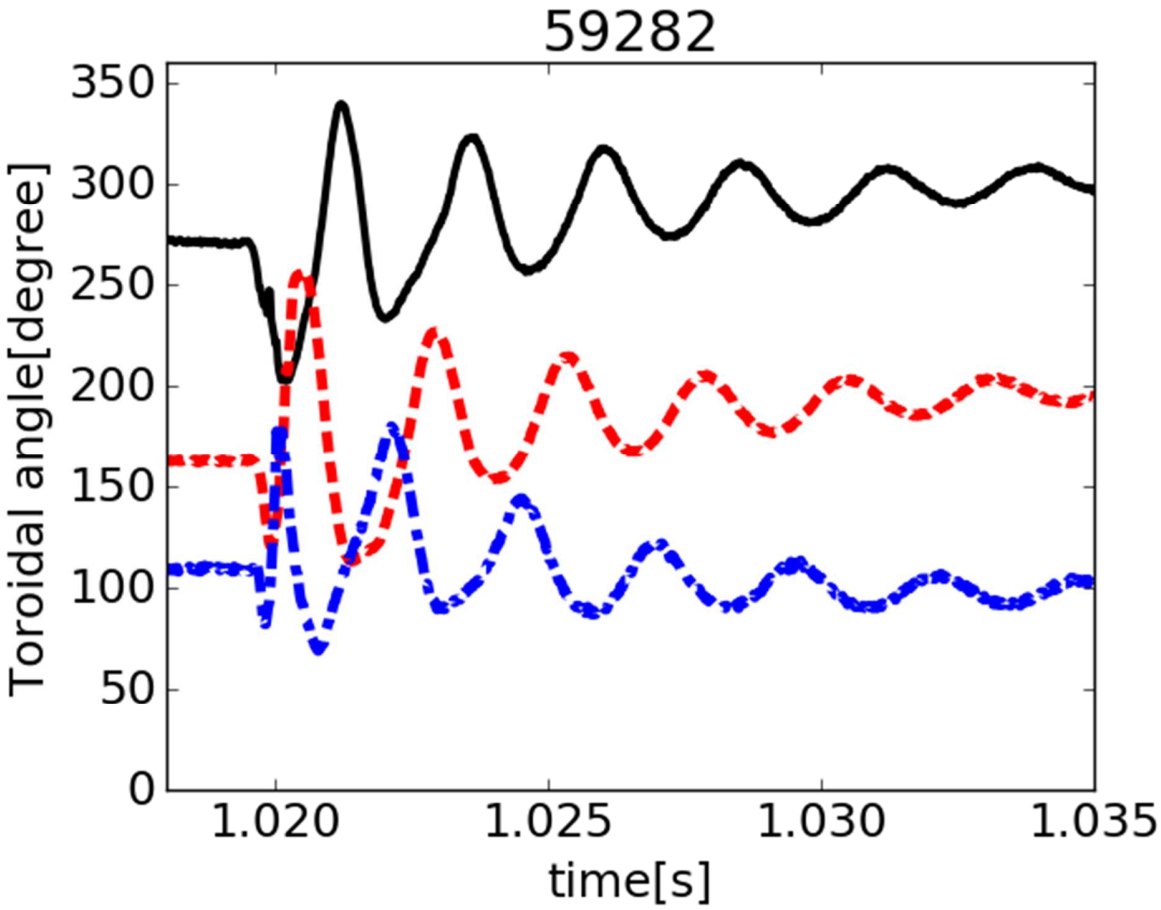

FIG. 6. SX emission signals from chords viewing around $\iota = 1$ surfaces at different toroidal angles, $\phi = 108$, 162 and 270 degrees, respectively. The thickness of Be foil installed in each SX diagnostic is 15 μm. This type-I oscillation is the same as that in Fig. 5.

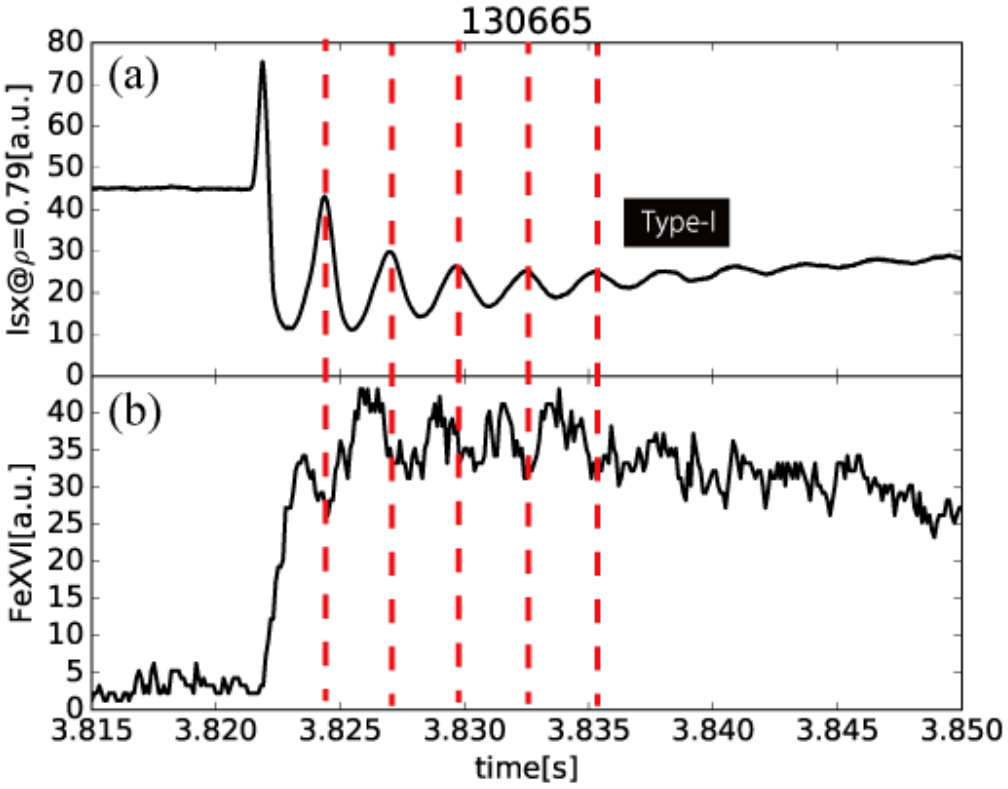

FIG. 7. (a) SX emission signal viewing around the $\iota = 1$ surface and (b) line emission of FeXVI measured by a spectrometer.

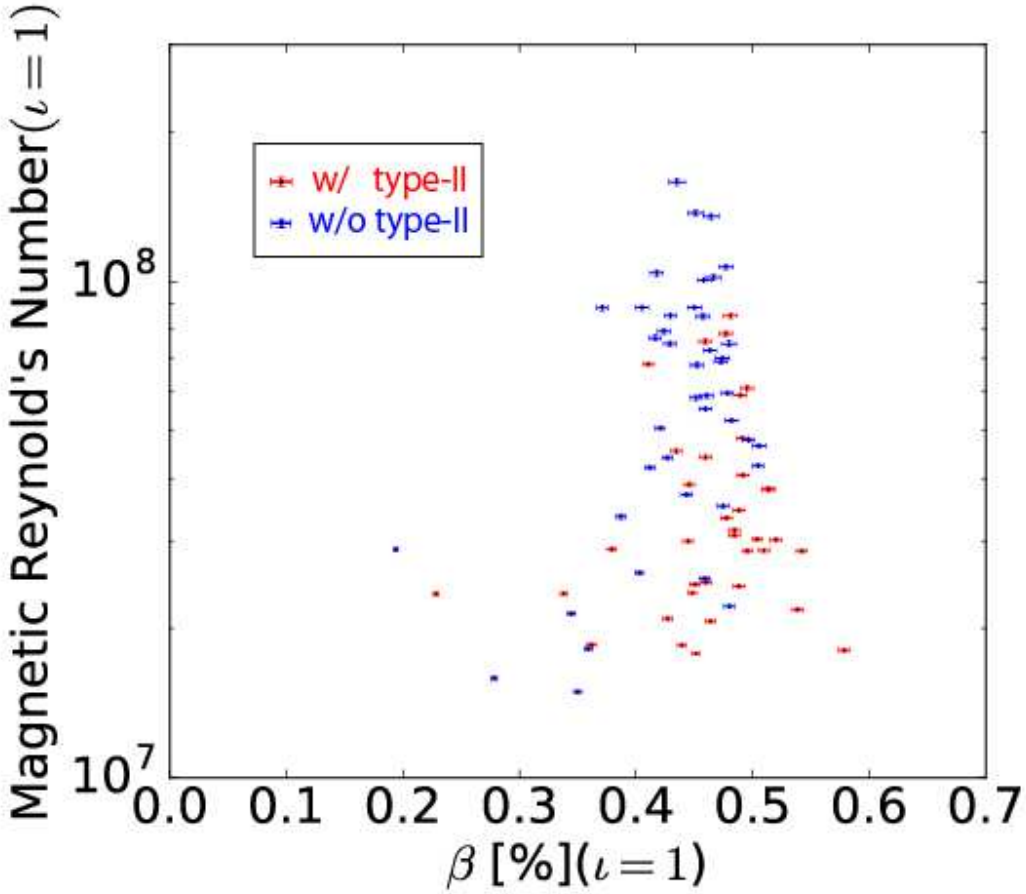

FIG. 8. Relationship between the magnetic Reynold's number, S, and the local β value around $\iota = 1$ surfaces obtained by Thomson scattering measurement with and without m/n = 1/1 mode where R_{ax} = 3.6 m, Bt = -2.75 T.

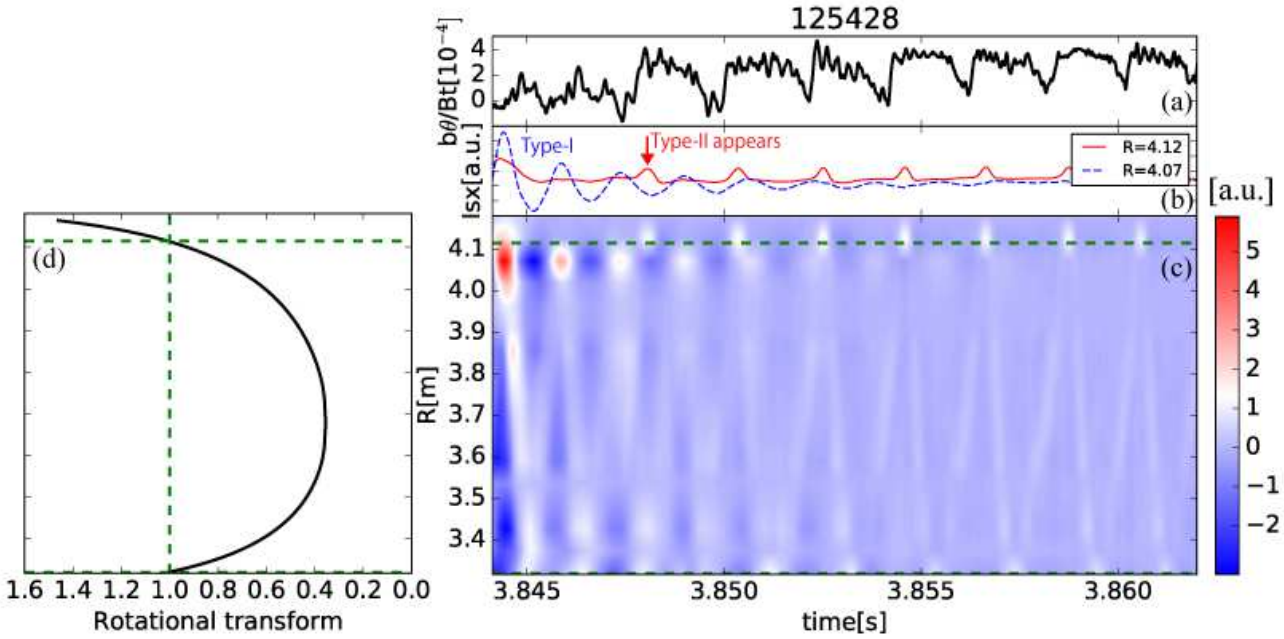

FIG. 9. Time evolution of (a) magnetic fluctuation, (b) SX emission signals, (c) fluctuation component of SX emission signals and (c) the ι profile when the snake-like oscillation and the resistive interchange mode appear at the same time.

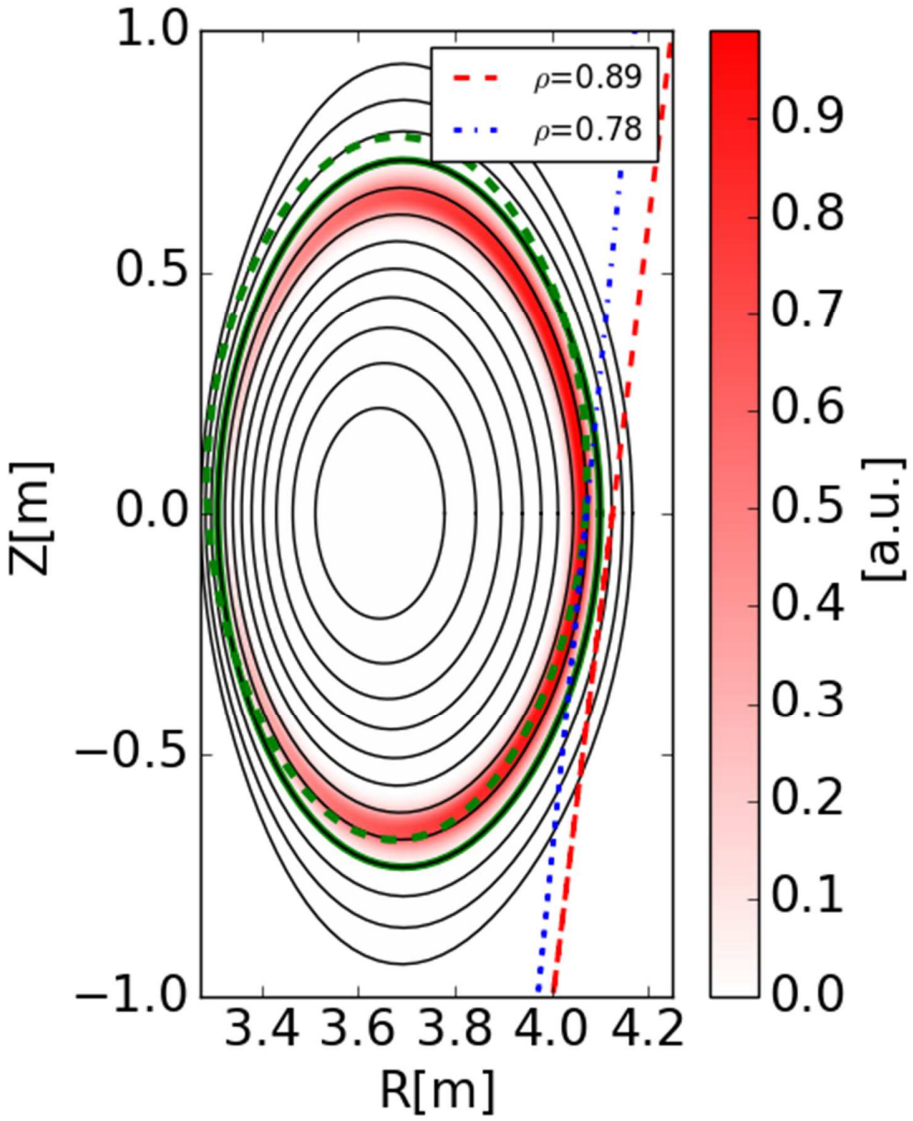

FIG. 10. The schematic drawing of the strong emission layer at a vertically elongated poloidal cross section with flux surfaces is illustrated. The solid green surface is the surface with $\iota = 1$, and the dashed green line is the deformed $\iota = 1$ surface with $m = 1$ deformation. The red and blue sight lines are for two signals in Fig. 3(a).